"Paddle-Wheel" Tris(cyclopentadienyl)tin(II) and -lead(II) Complexes: Syntheses, Structures, and Model MO Calculations

David R. Armstrong,[†] Melinda J. Duer,[‡] Matthew G. Davidson,[‡] David Moncrieff,*[,§] Christopher A. Russell,[‡] Clare Stourton,[‡] Alexander Steiner,[∥] Dietmar Stalke,[∥] and Dominic S. Wright*[,‡]

Department of Pure and Applied Chemistry, University of Strathclyde, Thomas Graham Building, 295 Cathedral Street, Glasgow, G1 1XL, U.K., Department of Chemistry, Lensfield Road, Cambridge CB2 1EW, U.K., Supercomputer Computations Research Institute B-186, Florida State University, Tallahassee, Florida 32306-4052, and Institut für Anorganische Chemie, Tammannstrasse 4, D-37077 Göttingen, Germany

Received February 28, 1997[⊗]

Nucleophilic addition reactions of cyclopentadienide anions (Cp^-) to bis(cyclopentadienyl)-tin(II) and -lead(II) produces complexes containing "paddle-wheel" $[(\eta^5\text{-}Cp)_3E]^-$ ($Cp = C_5H_5$; E = Sn, Pb) anions. Thus, the heavy main-group metals act as Lewis acids rather than as bases. The syntheses and X-ray structures of four such complexes, $[(\eta^5\text{-}Cp)_2Sn(\mu\text{-}Cp)\text{-}NaPMDETA]$ (**1**; PMDETA = $[(CH_3)_2NCH_2CH_2]_2NCH_3$), $[Mg(THF)_6]^{2+}[(\eta^3\text{-}Cp)_3Sn^-]_2$ (**2**), $[(\eta^5\text{-}Cp)_2Pb(\mu\text{-}Cp)NaPMDETA]$ (**3**), and $[Mg(THF)_6]^{2+}[(\eta^3\text{-}Cp)_3Pb^-]_2$ (**4**), are reported. The monomeric complexes **1** and **3** are essentially isostructural and contain trigonal-planar $(\eta^5\text{-}Cp)_3E$ units linked, through bridging $\mu\text{-}\eta^5$-Cp ligands, to $NaPMDETA^+$ cations in their molecular structures. *Ab initio* MO calculations have been used to probe the structures and charge distributions of the $[(\eta^5\text{-}Cp)_3E]^-$ anions in these complexes. These show that the natures of the species are highly dependent on the extent of alkali- or alkaline-earth-metal cation solvation. Thus, whereas unsolvated $[(\eta^5\text{-}Cp)_2E(\mu\text{-}Cp)Na]$ (E = Sn, Pb) are loose-contact complexes of $[Cp_2E]$ and [CpNa], $[(\eta^3\text{-}Cp)_3E]^-$ species are best formulated as triorganometal anions. Solid-state magic angle spinning (MAS) ^{119}Sn and ^{13}C NMR spectroscopic studies are in broad agreement with the model *ab initio* calculations and illustrate that in $[(\eta^5\text{-}Cp)_2Sn(\mu\text{-}Cp)NaPMDETA]$, in which partial solvation of the Na^+ coordination sphere occurs, the electronic situation approaches that in $[Cp_2Sn]$.

Introduction

Recently we have been interested in the nature of the interactions of heavy-p-block metals (E = group 13 (In, Tl), group 14 (Sn, Pb), group 15 (Sb, Bi)) with early-main-group metals (M = group 1 (Li, Na, etc.), group 2 (Mg, Ca, etc.)).[1a,2,3] These studies have led to the syntheses and characterization of the $[Ph_3E{-}LiPMDETA]$ complexes (E = Sn, Pb; PMDETA = $[(CH_3)_2NCH_2CH_2]_2NCH_3$), which contain the first structurally authenticated examples of bonds between early-main-group metals and heavy-p block metals.[1−3] All previously structurally characterized examples of triorganostannate or triorganoplumbate complexes had been ion-separated or else the early-main-group metal and the p-block metal were associated together by bridging heteroatoms (O, Cl, P) rather than by a direct bond.[4] The nature of this metal−metal (E−M) bonding appears to arise from *n*s and np_z interaction of the late-p-block metal with lithium.[2,3] The strength of this interaction dictates the deformation, toward or away from pyramidal, in the $[Ph_3E]^-$ anions involved.

Our exploration of the structures and properties of triorganostannate and plumbate complexes, which are valuable synthetic reagents in organic synthesis,[5] has most recently concerned the development of new synthetic routes. Previously such species have been prepared by the metalation of E−H or E−X (X = halogen) bonds or by the cleavage of E−E bonds with various metal sources.[5] We have shown that bis(cyclopentadienyl)tin(II) ($[Cp_2Sn]$, $Cp = C_5H_5$)[6] is a valuable and convenient precursor in the syntheses of these complexes.[7] Nucleophilic *addition* of sodium cyclopentadienide [CpNa] to $[Cp_2Sn]$ and PMDETA (1 equiv of each) yields the unprecedented $[(\eta^5\text{-}Cp)_2Sn(\mu\text{-}Cp)NaPMDETA]$ complex **(1)**. The complex contains an essentially

[†] University of Strathclyde.
[‡] Cambridge University.
[§] Florida State University.
[∥] Institute fur Anorganische Chemie.
[⊗] Abstract published in *Advance ACS Abstracts,* June 1, 1997.

(1) (a) Reed, D.; Stalke, D.; Wright, D. S. *Angew. Chem.* **1991**, *103*, 1539−1540; *Angew. Chem., Int. Ed. Engl.* **1991**, *30*. 1459. (b) Hitchcock, P. B.; Lappert, M. F.; Lawless, G. A.; Royo, B. *J. Chem. Soc., Chem. Commun.* **1993**, 554.

(2) Armstrong, D. R.; Davidson, M. G.; Moncrieff, D.; Stalke, D.; Wright, D. S. *J. Chem. Soc., Chem. Commun.* **1992**, 1413.

(3) Armstrong, D. R.; Moncrieff, D.; Stalke, D.; Wright, D. S. Unpublished results.

(4) A search of the Cambridge Crystallography Data Centre: Director, Dr. O. Kennard.

(5) (a) Pereyre, M.; Quintard, J.-P.; Rahm, A. *Tin in Organic Synthesis*; Butterworths: London, 1987. (b) Yamamoto, Y. Organotin Compounds in Organic Synthesis. *Tetrahedron* **1989**, *45*, 909. (c) Harrison, P. G. Chemistry of Tin; Chapman and Hall: New York, 1989. (d) Omae, I. *Organotin Chemistry*; Elsevier: Amsterdam, 1989.

(6) (a) Fischer, E. O.; Gruber, H. *Z. Naturforsch.* **1956**, *B11*, 423. (b) Almenningen, A.; Haaland, A.; Motzfeld, T. *J. Organomet. Chem.* **1967**, *7*, 97. (c) Atwood, J. L.; Hunter, W. E.; Cowley, A. H.; Jones, R. A. *J. Chem. Soc., Chem. Commun.* **1981**, 925.

(7) (a) Davidson, M. G.; Stalke, D.; Wright, D. S. *Angew. Chem.* **1992**, *104*, 1265; *Angew. Chem., Int. Ed. Engl.* **1992**, 31, 1226. (b) Edwards, A. J.; Paver, M. A.; Raithby. P. R.; Russell, C. A.; Stalke, D.; Steiner, A.; Wright, D. S. *J. Chem., Soc., Dalton Trans.* **1993**, 1465.

S0276-7333(97)00161-1 CCC: $14.00

Table 1. Crystal Data for [(η^5-Cp)$_2$Sn(μ-Cp)NaPMDETA] (1), [Mg(THF)$_6$]$^{2+}$[(η^3-Cp)$_3$Sn$^-$]$_2$ (2), [(η^5-Cp)$_2$Pb(μ-Cp)NaPMDETA] (3), and [Mg(THF)$_6$]$^{2+}$[(η^3-Cp)$_3$Pb$^-$]$_2$ (4)

	$C_{24}H_{38}N_3NaSn$ (**1**)	$C_{54}H_{78}O_6MgSn_2$·THF (**2**)	$C_{24}H_{38}N_3NaPb$ (**3**)	$C_{54}H_{78}O_6MgPb_2$·THF (**4**)
fw	510.25	1156.96	598.75	1333.96
cryst color, habit	light yellow, cubic rods	colorless, cubic	yellow, cubic	yellow, cubic
temp (K)	153(1)	153(2)	153(1)	153(1)
λ (Å)	0.710 73	0.710 73	0.710 73	0.710 73
cryst dimens (mm)	0.55 × 0.5 × 0.4	0.4 × 0.3 × 0.3	0.3 × 0.3 × 0.3	0.3 × 0.2 × 0.2
cryst syst	monoclinic	rhombohedral	monoclinic	rhombohedral
space group	$P2_1/c$	$R\bar{3}$	$P2_1/c$	$R\bar{3}$
lattice params				
a (Å)	8.713(2)	14.472(2)	8.7561(9)	14.505(2)
b (Å)	17.221(3)	14.472(2)	17.264(3)	14.505(2)
c (Å)	16.345(3)	22.811(5)	16.341(3)	22.769(5)
α (deg)	90.0	90.0	90.0	90.0
β (deg)	96.61(3)	90.0	96.66(2)	90.0
γ (deg)	90.0	120.0	90.0	120.0
V_{cell} (Å^3)	2436.2(8)	4137.4(12)	2453.5(8)	4148.7(12)
Z	4	3	4	3
D_{calcd} (Mg m^{-3})	1.392	1.393	1.621	1.602
μ(Mo Kα) (mm^{-1})	1.081	0.967	6.908	6.140
θ range (deg)	4.20−30.13	4.39−25.99	3.23−25.33	4.38−29.98
no. of rflns collected	10 529	7959	4119	5290
no. of indep rflns	7091	1804	3974	2685
R indices (all data) ($F > 4\sigma(F)$)[a]	R1 = 0.021, wR2 = 0.048	R1 = 0.016, wR2 = 0.039	R1 = 0.041, wR2 = 0.086	R1 = 0.041, wR2 = 0.099
R indices (all data)[a]	R1 = 0.026, wR2 = 0.050	R1 = 0.017, wR2 = 0.039	R1 = 0.063, wR2 = 0.106	R1 = 0.047, wR2 = 0.101
peak and hole (e Å^{-3})	+ 0.386, −0.332	+0.266, −0.245	1.295, −1.840	3.019, 1.986

[a] R1 = $\Sigma|F_o - F_c|/\Sigma F_o$ and wR2 = $(\Sigma w(F_o^2 - F_c^2)^2/\Sigma w(F_o^2)^2)^{0.5}$; $w = 1/[\sigma^2(F_o^2) + (xP)^2 + yP]$, $P = F_o^2 + 2F_c^2/3$.

trigonal-planar paddle-wheel [Cp$_3$Sn]$^-$ ion in the solid state and in solution.[7a] The existence of this anion, rather than the [(η^5-Cp)$_2$Sn(μ-Cp)Na] fragment of **1** arising simply through loose association of [Cp$_2$Sn] and [CpNa], is proved conclusively by the observation of an ion-separated [Cp$_3$Sn]$^-$ anion in the structure of [Mg(THF)$_6$]$^{2+}$[(η^3-Cp)$_3$Sn$^-$]$_2$ **(2).**[7b] The essentially planar geometries of the [Cp$_3$Sn]$^-$ anions of **1** and **2** are unique among the structures of triorganstannates; all others contain nearly *pyramidal* [R$_3$Sn]$^-$ anions.[1−4,7b] We report here a full account of this work and, for the first time, the syntheses and structures of the lead analogues [(η^5-Cp)$_2$Pb(μ-Cp)NaPMDETA] **(3)** and [Mg(THF)$_6$]$^{2+}$[(η^3-Cp)$_3$Pb$^-$]$_2$ **(4)**. *Ab initio* MO calculations on unsolvated and Lewis base solvated models of **1**−**4** and solid-state ^{119}Sn and ^{13}C MAS NMR studies of **1** and **2** have been used to probe the nature of the interactions of the Cp ligands with Sn and Pb in these complexes. These studies show that solvation of the s-block metal cations strongly influences the charge distribution in these complexes.

Results and Discussion

Syntheses and Structures of 1−4. The reactions of [CpNa] and [Cp$_2$Mg] with Cp$_2$Sn,[6] producing [(η^5-Cp)$_2$Sn(μ-Cp)NaPMDETA] **(1)**[7a] and [Mg(THF)$_6$]$^{2+}$[(η^3-Cp)$_3$Sn$^-$]$_2$ **(2)**[7b] respectively, and of [CpNa] and [Cp$_2$Mg] with Cp$_2$Pb,[8] producing (η^5-Cp)$_2$Pb(μ-Cp)NaPMDETA **(3)** and [Mg(THF)$_6$]$^{2+}$.[η^3-Cp$_3$Pb$^-$]$_2$ **(4)**, all occur rapidly and smoothly at room temperature with little or no decomposition into Sn or Pb (see Experimental Section). Indeed, all the complexes appear to be extremely thermally stable (melting without decomposition in the range of 57 °C for **2** to 146 °C for **3**). Basic characterization of all the products was obtained by a combination of elemental analyses (C, H, N) and infrared and ^{1}H NMR spectroscopy. Cryoscopic molecular mass measurements (in benzene) were used in combination with variable-temperature ^{1}H NMR spectroscopy to probe the solution behavior of these complexes where soluble.

Table 2. Selected Bond Lengths (Å) and Bond Angles (deg) for (η^5-Cp)$_2$Sn(μ-Cp)NaPMDETA (1)

Sn(1)−C(1)	2.922(2)	C(4)−C(5)	1.398(2)
Sn(1)−C(2)	2.881(2)	C(5)−C(1)	1.396(2)
Sn(1)−C(3)	3.004(2)	C(6)−C(7)	1.400(2)
Sn(1)−C(4)	3.107(2)	C(7)−C(8)	1.394(2)
Sn(1)−C(5)	3.059(2)	C(8)−C(9)	1.410(2)
Sn(1)−Cp(A)	2.75	C(9)−C(10)	1.394(2)
Sn(1)−C(6)	2.761(2)	C(10)−C(6)	1.410(2)
Sn(1)−C(7)	2.865(2)	C(11)−C(12)	1.399(2)
Sn(1)−C(8)	2.905(2)	C(12)−C(13)	1.385(3)
Sn(1)−C(9)	2.841(2)	C(13)−C(14)	1.389(3)
Sn(1)−C(10)	2.742(2)	C(14)−C(15)	1.399(3)
Sn(1)−Cp(B)	2.56	C(15)−C(11)	1.380(3)
Sn(1)−C(11)	2.802(2)	Na(1)−C(1)	2.782(2)
Sn(1)−C(12)	2.880(2)	Na(1)−C(2)	2.800(2)
Sn(1)−C(13)	2.851(2)	Na(1)−C(3)	2.830(2)
Sn(1)−C(14)	2.739(2)	Na(1)−C(4)	2.846(2)
Sn(1)−C(15)	2.713(2)	Na(1)−C(5)	2.813(2)
Sn(1)−Cp(C)	2.53	Na(1)−Cp(A)	2.55
C(1)−C(2)	1.403(2)	Na(1)−N(1)	2.565(2)
C(2)−C(3)	1.394(2)	Na(1)−N(2)	2.538(2)
C(3)−C(4)	1.396(2)	Na(1)−N(3)	2.464(2)

Sn(1)−Cp(A)−Na(1)	172.3	Cp(B)−Sn(1)−Cp(C)	124.0
Cp(A)−Sn(1)−Cp(B)	116.3	Cp(C)−Sn(1)−Cp(A)	118.9

1−**4** were finally fully characterized by obtaining their crystal structures at low temperature (153 K). Details of these structural analyses are given in Table 1, and selected bond lengths and bond angles within complexes **1**−**4** are collected in Tables 2−5, respectively.

The structure of **1** is monomeric (Figure 1a). It contains an [(η^5-Cp)$_3$Sn]$^-$ paddle-wheel triorganostannate anion in which one Cp is additionally involved in a [Sn(μ-Cp)Na] bridge. The Sn center is nearly trigonal planar (average Cp(centroid)−Sn−Cp(centroid), 119.7(1)°;

(8) (a) Fischer, E. O.; Gruber, H. *Z. Anorg. Allg. Chem.* **1956**, *286*, 237. (b) Pannattoni, J. C.; Bombieri, G.; Croatto, U. *Acta Crystallogr.* **1966**, *21*, 823.

Table 3. Selected Bond Lengths (Å) and Bond Angles (deg) for $[(\eta^3\text{-Cp})_3Sn^-]_2[Mg(THF)_6]^{2+}$ (2)

Sn(1)−C(1)	2.621(2)	C(1)−C(2)	1.410(2)
Sn(1)−C(2)	2.862(2)	C(2)−C(3)	1.390(2)
Sn(1)−C(3)	3.066(2)	C(3)−C(4)	1.404(2)
Sn(1)−C(4)	3.092(2)	C(4)−C(5)	1.390(2)
Sn(1)−C(5)	2.805(2)	C(1)−C(5)	1.414(3)
Sn(1)−Cp	2.65	Mg(1)−O (av)	2.094(1)
Cp−Sn−Cp	118.8	O−Mg−O	89.77(4)−90.22(4)

Table 4. Selected Bond Lengths (Å) and Bond Angles (deg) for $[(\eta^5\text{-Cp})_2Pb(\mu\text{-Cp})NaPMDETA]$ (3)

Pb(1)−C(1)	2.94(1)	Pb(1)−C(13)	2.833(9)
Pb(1)−C(2)	3.04(1)	Pb(1)−C(14)	2.90(1)
Pb(1)−C(3)	3.06(1)	Pb(1)−C(15)	2.95(1)
Pb(1)−C(4)	3.00(1)	Pb(1)−Cp(C)	2.63
Pb(1)−C(5)	2.91(1)	Cp C ·· C	1.38(1)−1.42(1)
Pb(1)−Cp(A)	2.74	Na(1)−C(1)	2.777(9)
Pb(1)−C(6)	2.92(1)	Na(1)−C(2)	2.800(2)
Pb(1)−C(7)	2.90(1)	Na(1)−C(3)	2.83(1)
Pb(1)−C(8)	2.82(1)	Na(1)−C(4)	2.88(1)
Pb(1)−C(9)	2.79(1)	Na(1)−C(5)	2.84(1)
Pb(1)−C(10)	2.87(1)	Na(1)−Cp(A)	2.56
Pb(1)−Cp(B)	2.60	Na(1)−N(1)	2.467(8)
Pb(1)−C(11)	2.92(1)	Na(1)−N(2)	2.554(8)
Pb(1)−C(12)	2.830(9)	Na(1)−N(3)	2.573(8)
Pb(1)−Cp(A)−Na(1)	172.9	Cp(B)−Pb(1)−Cp(C)	122.7
Cp(A)−Pb(1)−Cp(B)	119.7	Cp(C)−Pb(1)−Cp(A)	116.8

Table 5. Selected Bond Lengths (Å) and Bond Angles (deg) for $[(\eta^3\text{-Cp})_3Pb^-]_2Mg(THF)_6^{2+}$ (4)

Pb(1)−C(1)	2.711(5)	C(1)−C(2)	1.415(8)
Pb(1)−C(2)	2.840(5)	C(2)−C(3)	1.390(8)
Pb(1)−C(3)	3.066(5)	C(3)−C(4)	1.396(8)
Pb(1)−C(4)	3.097(5)	C(4)−C(5)	1.387(8)
Pb(1)−C(5)	2.905(5)	C(1)−C(5)	1.396(8)
Pb(1)−Cp	2.68	Mg(1)−O	2.087(3)
Cp−Pb−Cp	118.8	O−Mg−O	89.9(1)−90.1(1)

Sn only *ca.* 0.14 Å out of the plane of the three Cp centers). The overall structure of **1** can be rationalized in terms of the competition by the Sn and Na centers for the electron density on the bridging Cp ligand, through the slightly bent [Sn(μ-Cp)Na] bridge (Sn(1)−Cp(A)−Na(1), 172.3°). This competition lengthens the μ-Cp contact with Sn (Cp(A)−Sn(1), 2.75 Å) compared to those made with the terminally attached Cp ligands (average Cp(B,C)−Sn(1), 2.54 Å; cf. Sn−Cp, average *ca.* 2.42 Å in Cp_2Sn[6c]).

The deviation from linearity of the Sn(μ-Cp)Na bridge appears to be almost entirely a consequence of crystal packing. The Na atom is almost perpendicular (88.30(1)°) to the Cp(A) ring plane in its contact to the Cp centroid (Cp(A)−Na(1), 2.55 Å; cf. (μ-Cp)−Na in polymeric [(μ-Cp)Na.TMEDA]$_\infty$, *ca.* 2.65 Å,[9] and Cp*−Na (Cp* = $C_5(CH_3)_5$) in molecular [(η^5-Cp*)Na(pyridine)$_3$], 2.40 Å[10]). This bending of the Sn(μ-η^5-Cp)Na bridge is caused by two long-range intermolecular C(H)···Na interactions (H···Na(1), *ca.* 3.15 and 3.49 Å) with the $Na(PMDETA)^+$ unit. These interactions link monomers of **1** into a loose polymeric array (Figure 1b).

Although a number of early-main-group-metal stannates have been structurally characterized, only [Ph_3-Sn−LiPMDETA][1a] and [$(Me_2CH)_3$Sn−K(η^6-toluene)$_3$][1b] contain alkali-metal−Sn bonds. The role of the μ-Cp ligand in **1**, in holding the Sn and Na centers together, is comparable with that of bridging heteroatoms (e.g., O, P, Cl) in other stannate complexes, e.g., O in Li(μ-$Ph_2C_6H_3O)_3Sn$.[11a] The planar geometry of the Sn in **1** is unprecedented in the structures of triorganostanates. All other complexes of this type, whether ion-separated[4,11b] or ion-contacted,[1] have nearly pyramidal stannnate ions. The geometry of the Sn center in **1** implies a very different use of orbitals than in other stannates. Complex **1** is rare among Sn(II) organometallics in containing three π-bonded aromatic ligands bonded to Sn. Polymerically linked [(η^5-Cp)$_3$Sn−X] units (X = μ-F−BF_3^- and THF) have been seen in the structure of {BF_4^-[(η^5-Cp)$_2$Sn(μ-Cp)Sn(THF)]$^+$}$_\infty$, produced by the reaction of BF_3 with [Cp_2Sn] in THF (Cp−Sn, *ca.* 2.29−3.67 Å).[12]

Cryoscopic molecular mass measurements in benzene show that two solution species are present over a range of concentrations [{(η^5-Cp)$_2$Sn(μ-Cp)NaPMDETA]$_n$; n = 0.49 ± 0.02 (0.015 mol L^{-1}), 0.51 ± 0.02 (0.030 mol L^{-1})). ^{1}H NMR spectra of **1** at +25 °C (400MHz, d_8-toluene) shows just one sharp signal at δ 5.97 due to the Cp ligands. There are no signals below this which could be attributed to [CpNa]. Reducing the temperature (*ca.* −40 °C) results in splitting of the η^5-Cp signal. Eventually (*ca.* −80 °C) these two resonances are fully resolved at a ratio of 2:1: δ 6.02 (η^5-Cp, $^2J_{Sn-H}$, 29.4 Hz) and δ 6.00 (μ-Cp, $^2J_{Sn-H}$, 28.8 Hz) (Figure 1c). Although the nature of the species present in solutions of **1** at room temperature is uncertain (i.e., whether they are [Cp_2Sn]/[CpNaPMDETA] or [Cp_3Sn]$^-$/[NaPMDETA]$^+$), the complex appears to be ion-paired at low temperature (i.e., the same structure as that occurring in the solid state).

The structure of $[Mg(THF)_6]^{2+}[(\eta^3\text{-Cp})_3Sn^-]_2$ **2** (Figure 2) contains an ion-separated [(η^3-Cp)$_3$Sn]$^-$ anion. There is one THF molecule per formula unit in the crystal lattice which is removed when the complex is placed under vacuum (*ca.* 10^{-2} atm, 15 min). The observation of separate [(η^3-Cp)$_3$Sn]$^-$ ions in **2** verifies that this anion has a true existence. The Cp ligands of the anion are bound equivalently to the Sn center (Cp−Sn(1), 2.65 Å). The Cp(centroid)−Sn contacts are significantly shorter than those found in **1**. There is also a distortion in the anion geometry away from the almost planar geometry of the ion-contacted [(η^5-Cp)$_3$Sn] unit in **1** toward a more pyramidal geometry in the ion-separated [(η^3-Cp)$_3$Sn]$^-$ anions of **2** (Sn *ca.* 0.29 Å out of the Cp(centroid) mean plane, cf. only 0.14 Å in **1**). The more pyramidal geometry of the ion-separated anion in **2** is analogous to the situation occurring in ion-separated and Sn−Li-contacted [Ph_3Sn]$^-$ complexes, where the separated anions have a slightly more pyramidal geometry than the contacted ones.[1,3,11b] This change in geometry of the [Cp_3Sn]$^-$ anion in **2** and in the hapticity of the Cp ligands from η^5 in **1** to η^3 in **2** presumably reflects an increase in lone-pair character on Sn. The octahedral coordination geometry in the $[Mg(THF)_6]^{2+}$ cation of **2** is unremarkable.[13]

Unfortunately, complex **2** proved to be too insoluble in benzene to allow cryoscopic investigations. However,

(9) Aoyagi, T.; Shearer, H. M. M.; Wade, K.; Whitehead, G. *J. Organomet. Chem.*, **1979**, *175*, 21.

(10) Rade, G.; Roesky, H. W.; Stalke, D.; Pauer, F.; Sheldrick, G. M. *J. Organomet. Chem.* **1991**, *403*, 11.

(11) (a) Smith, G. D.; Fanwick, P. E.; Rothwell, I. P. *Inorg. Chem.* **1989**, *26*, 618. (b) Birchall, T.; Vetrone, J. A. *J. Chem. Soc., Chem. Commun.* **1988**, 877.

(12) Dory, T. S.; Zuckerman, J. J.; Barnes, C. L. *J. Organomet. Chem.* **1985**, *281*, C1.

(13) (a) Poonia, N. S.; Bajaj, A. V. *Chem. Rev.* **1979**, *79*, 389. (b) Poonia, N. S.; Bajaj, A. V. *Chem. Rev.* **1988**, *87*, 55.

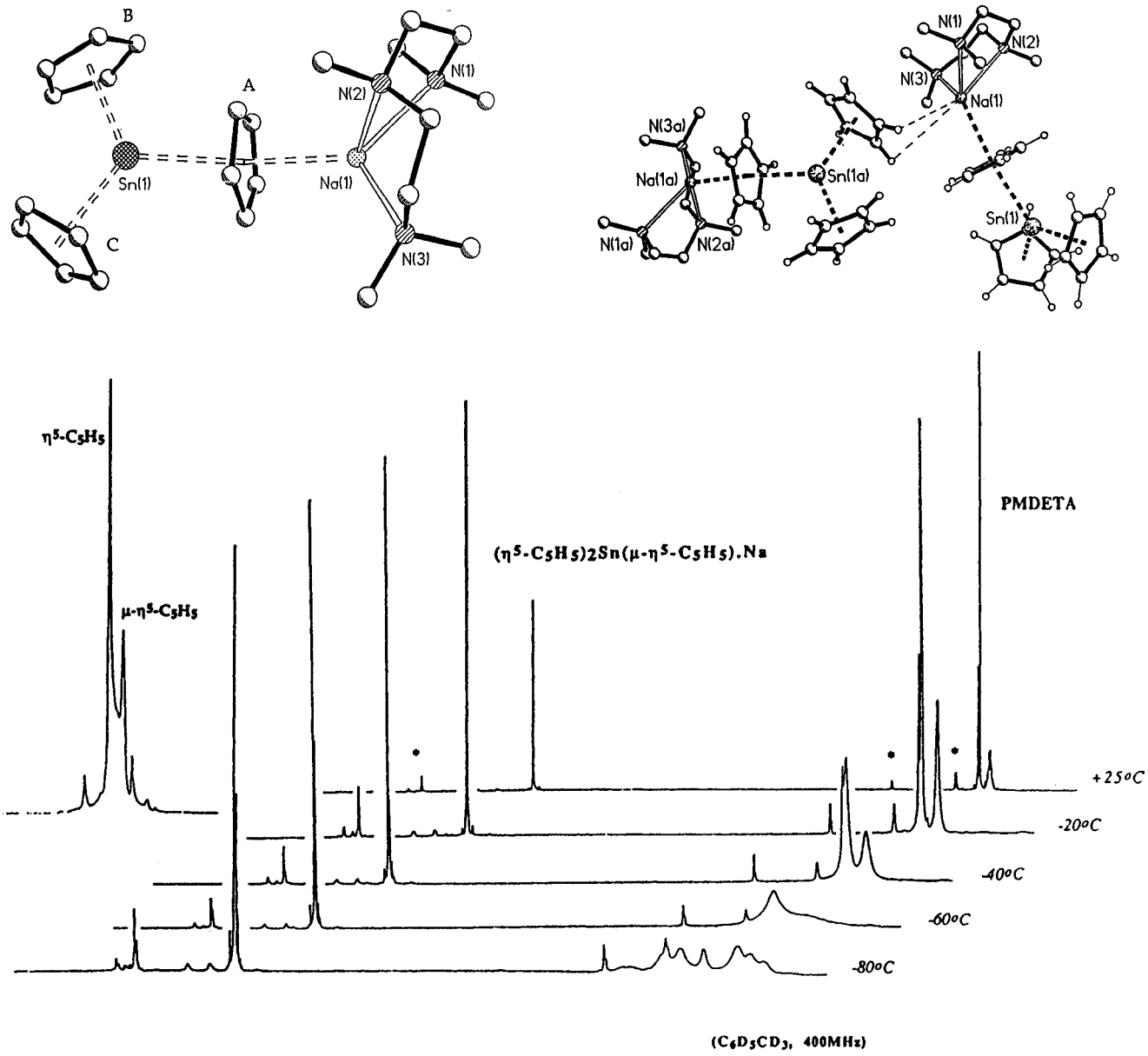

Figure 1. (a, top left) Molecules of **1** in the asymmetric unit. Hydrogen atoms have been omitted for clarity. For key bond lengths and angles see, Table 2. (b, top right) Packing diagram showing the intermolecular C−H···Na interactions between molecules of **1** (see Table 2). (c, bottom) Variable-temperature ^{1}H NMR study of **1** in d_8-toluene (400.16 MHz).

variable-temperature high-field ^{1}H NMR studies (360.14 MHz) indicate that **2** has an ion-separated structure in solution similar to that occurring in the solid state. The Cp resonance (δ 5.77) remains a singlet even down to −85 °C with essentially no change in its position with changing temperature.

[(η^5-Cp)$_2$Pb(μ-Cp)NaPMDETA] **(3)** is almost isostructural with the ion-contacted Sn complex **1** (Figure 3). Thus, the structure is composed of an almost planar [(η^5-Cp)$_3$Pb]$^-$ anion (Pb(1) 0.14 Å out of the mean plane) linked, through a μ-Cp bridge, to a [Na(PMDETA)]$^+$ cation. The role of the μ-Cp ligand in **3**, in holding the Pb and Na centers together, is comparable with that of bridging (O and P) heteroatoms in the few structurally characterized plumbate complexes, e.g., P in [^{t}Bu$_2$PPb-(μ-P^{t}Bu$_2$)$_2$Li.THF].[14] A trigonal-planar geometry for Pb has also been seen in the solid-state structure of the {[Cp′(CO)$_2$Mn]$_2$Pb.S^{t}Bu}$^-$ (Cp′ = C$_5$H$_4$Me) anion.[15] The Cp ligands of **3** are bound to Pb at distances similar to those in the Sn analogue **1** (Cp(B,C)−Pb(1), average 2.62 Å; Cp(A)−Pb(1), 2.74 Å). The C−Pb distances to the bridging Cp ligand are slightly shorter (average 2.99 Å) and the terminal C−Pb distances are slightly longer (average 2.87 Å) than the bridging and terminal Cp C−Pb bond lengths in the polymeric structure of [Cp$_2$Pb]$_\infty$ (cf. bridging (3.06 Å), terminal (2.76 Å), and average (2.78 Å)[8b] in the gas-phase structure of the monomer[6b]). The Pb(μ-Cp)Na bridge in **3** is also bent (172.9°), and the complex is linked into a polymeric array by long-range intermolecular H···Na interactions in a manner similar to that for **1** (H···Na(1), *ca.* 3.0 and 3.4 Å).

The ion-separated structure of [Mg(THF)$_6$]$^{2+}$[(η^3-Cp)$_3$-Pb$^-$]$_2$ **(4)** (Figure 4) is almost isostructural with the Sn analogue **2**. There is also lattice solvation by one molecule of THF per formula unit which, like **2**, is

(14) Arif, A. M.; Cowley, A. H.; Jones, R. A.; Power, J. M. *J. Chem. Soc., Chem. Commun.* **1986**, 1446.

(15) Huttner, F. E. G.; Zsolnai, L. *Angew. Chem.* **1989**, *101*, 1525; *Angew. Chem., Int. Ed. Engl.* **1989**, *28*, 1496.

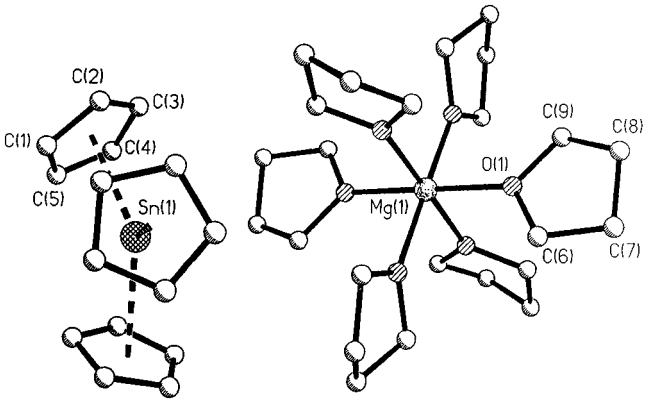

Figure 2. Molecules of **2** in the asymmetric unit (only one of the $[(\eta^3\text{-Cp})_3\text{Sn}]^-$ anions is shown). Hydrogen atoms and the lattice-bound THF have been omitted for clarity. For key bond lengths and angles, see Table 3.

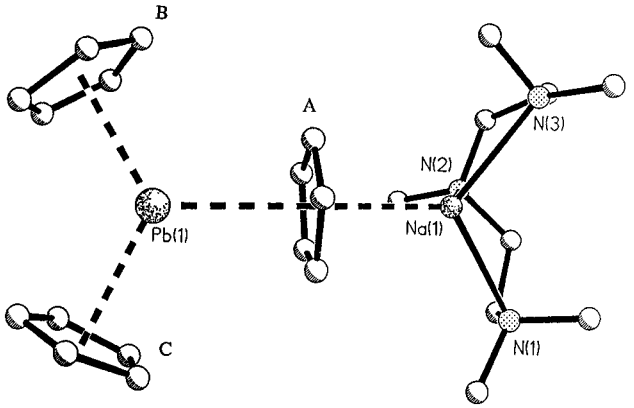

Figure 3. Molecules of **3** in the asymmetric unit. Hydrogen atoms have been omitted for clarity. For key bond lengths and angles see Table 4.

displaced by placing the complex under vacuum (*ca.* 10^{-2} atm, 15 min). Similar comparisons can be made between the ion-contacted and ion-separated Pb complexes (**3** and **4**, respectively) as were made earlier for the corresponding Sn compounds. There is again a switch to a less planar geometry in the ion-separated $[\text{Cp}_3\text{Pb}]^-$ anion compared to the ion-contacted Pb complex **3** (in **4** *ca.* 0.30 Å out of the Cp mean plane, cf. 0.14 Å in **3**) and a shift in hapticity of the Cp ligands from η^5 in **3** to η^3 in **4**. It is noticeable that the Pb in the ion-separated $[(\eta^3\text{-Cp})_3\text{Pb}]^-$ anion of **4** is less slipped from ideal η^5 geometry than the Sn in the ion-separated $[(\eta^3\text{-Cp})_3\text{Sn}]^-$ anion of **2**. This is shown graphically in Figure 4b, where the attachment of the Cp ligands in both complexes is compared in a view of the metal atoms perpendicular to the Cp ring plane.

Complexes **3** and **4** are some of the only π complexes of Pb to be characterized in the solid state and are rare examples containing three ligands π-bonded to Pb. In orthorhombic $[\text{Cp}_2\text{Pb}]_\infty$, $[(\mu\text{-Cp})_2(\eta^5\text{-Cp})\text{Pb}]$ units akin to the $[(\eta^5\text{-Cp})_3\text{Pb}]$ units of both complexes are present within its polymeric zigzag structure (average Cp−Pb, *ca.* 2.64 Å).[8b] The $[\text{Cp}_3\text{Pb}]$ units of **3** and **4** can be viewed as fragments of the $[\text{Cp}_2\text{Pb}]_\infty$ lattice. The observation of ion-separated $[(\eta^3\text{-Cp})_3\text{Pb}]^-$ units in **4** suggests that when $[\text{Cp}_2\text{Pb}]$ is dissolved in ether solvents $[\text{Cp}_3\text{Pb}^-\text{CpPb(ether)}_x]^+$ is the most likely solution species, rather than PbCp^+ cations and "bare" Cp^- anions, as has been proposed.[16]

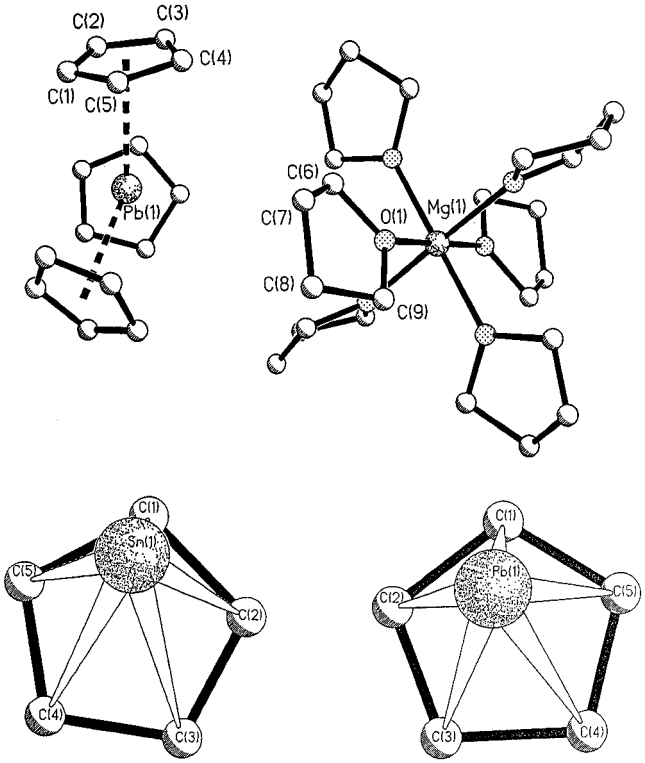

Figure 4. (a, top) Molecules of **4** in the asymmetric unit (only one of the $[(\eta^3\text{-Cp})_3\text{Pb}]^-$ anions is shown). Hydrogen atoms and the lattice-bound THF have been omitted for clarity. For key bond lengths and angles, see Table 5. (b, bottom) View of the η^3-Cp Sn and Pb linkages perpendicular to the Cp mean planes in **2** and **4**.

Finally, the solution dynamics of complexes **3** and **4** were investigated by cryoscopy and variable-temperature ^{1}H NMR. The poor solubility of **3** in benzene restricted cryoscopic measurements, and only low concentrations could be investigated. These results appeared to indicate initially that a dissociative equilibrium similar to that observed for the Sn analogue **1** is occurring for **3** ($n = 0.47 \pm 0.04$ (approximately saturated solution), 0.005mol L^{-1}). However, even room-temperature ^{1}H NMR (250 MHz) spectra of **3** in benzene exhibit two narrowly split Cp resonances at δ 5.28 and 5.27. This could suggest that **3** is dissociated into the neutral fragments ($[\text{Cp}_2\text{Pb}]_\infty$ (cf. δ 6.14 in THF at room temperature) and [CpNaPMDETA]) at room temperature. Low-temperature high-field NMR studies on **3** in toluene gave no further information concerning the nature of the equilibrium occurring here, and the resonances only broaden with reduced temperature (down to *ca.* −90 °C). For the ion-separated complex **4** the situation appears to be more simple. Although **4** has low solubility in benzene and therefore was not accessible to cryoscopic work, variable-temperature ^{1}H NMR studies imply simple dissociation of **4** into $[\text{Cp}_3\text{Pb}]^-$ and $[\text{Mg(THF)}_6]^{2+}$ ions is occurring in a manner identical with that for the Sn analogue **2**; only a singlet Cp resonance is observed for temperatures down to *ca.* −90 °C in toluene (δ 5.56).

Calculations. *Ab initio* calculations were performed on model compounds of tin and lead to examine the nature of bonding in the compounds **1**−**4**. The basis set

(16) Strohmeier, W.; Lansfeld, H.; Gernet, F. *Z. Electrochem.* **1962**, *66*, 823−827.

Table 6. Total Energies of Calculational Models of [Cp_2Sn], [Cp_2Pb], and [Cp_2Ge] by LANL1DZ Basis Set

compd (sym conformation[a]), real energy (kcal mol^{-1})	total energy (au)
[Cp_2Sn] (C_{2v}; h, h), 0.00	−387.577 757
[Cp_2Sn] (C_s; t, h), 0.00	−387.577 754
[Cp_2Sn] (C_{2v}; t, t), 0.43	−387.577 073
[Cp_2Sn] (D_{5d}), 4.00	−387.571 380
[Cp_2Sn] (D_{5h}), 4.00	−387.571 363
[Cp_2Pb] (C_{2v}; h, h), 0.00	−387.687 833
[Cp_2Pb] (C_s; t, h), 0.00	−387.687 829
[Cp_2Pb] (C_{2v}; t, t), 0.03	−387.687 787
[Cp_2Pb] (D_{5d}), 0.66	−387.686 775
[Cp_2Pb] (D_{5h}), 0.66	−387.686 765
[Cp_2Ge] (C_{2v}; h, h), 0.00	−387.937 091
[Cp_2Ge] (C_s; t, h), 0.00	−387.937 091
[Cp_2Ge] (C_{2v}; t, t), 1.44	−387.934 784
[Cp_2Ge] (D_{5d}; h, h), 6.43	−387.926 839
[Cp_2Ge] (D_{5h}; h, h), 6.43	−387.926 816

[a] t (toe) indicates that the C−H bond of one Cp ring coincident with the plane of symmetry is pointing toward the other Cp ring; h (heel) indicates that the C−H bond of one Cp ring coincident with the plane of symmetry is pointing away from the other Cp ring.

initially used for the tin and lead compounds was an effective core potential (ECP) double-ζ basis set (LANL1DZ)[17] dealing with the valence electrons only. It was found that it was impossible to achieve optimization for [$Cp_2Sn(\mu$-Cp)Na]. Hence, a second ECP basis set (SBKJC)[18] was also employed for the tin compounds. This consisted of a double-ζ representation of the valence orbitals of tin plus an extra set of sp orbitals of exponent 0.024 and a set of d orbitals of exponent 0.065. The orbitals of the other atoms were represented by the 6-311G** basis set.[19] The calculations were performed using the computer programs Gaussian92[20] and Gaussian94.[21]

The initial calculations using the LANL1DZ basis set focused on the geometry-optimized structures of the [Cp_2E] species (E = Sn, Pb). The resulting energies are presented in Table 6. The most stable configuration for both bis(cyclopentadienyl)tin and -lead was found to have a bent-sandwich structure where the rings are eclipsed with respect to each other. The C−H bonds of the Cp rings coincident with the plane of symmetry are pointing away from the other Cp ring, giving an overall symmetry of C_{2v}. This arrangement is found to be almost identical in energy with that of other bent structures where the rings are staggered with respect to each other, giving C_s symmetry, and marginally more stable than a third bent structure which also has C_{2v} symmetry but where the C−H bonds coincident with the plane of symmetry are pointing toward the other ring. The linear D_{5h} and D_{5d} models for [Cp_2E] are less stable than the bent structures, with an energy difference of 4.0 kcal mol^{-1} for [Cp_2Sn] and 0.7 kcal mol^{-1} for [Cp_2Pb]. The gas-phase structure determinations of stannocene[6b] and plumbocene[8b] show a bent-sandwich arrangement. Comparison between the experimental and calculated bond lengths and angles reveals similar features. The calculated perpendicular distances from the metal to the cyclopentadienyl ring planes for the ECP-generated geometries are 2.45 Å for [Cp_2Sn] and 2.56 Å for [Cp_2Pb], in reasonable agreement with the experimental values of 2.38−2.42[6b] and 2.50 Å,[8b] respectively. The geometry-optimized structures also reveal that metal slippage from the ring centroid position has also occurred with slippage distances of 0.67 and 0.34 Å for [Cp_2Sn] and [Cp_2Pb], respectively. The value for [Cp_2Sn] is somewhat greater than the corresponding experimental values, which range from 0.21 to 0.36 Å. The angles between the planes of the Cp rings are calculated to be 64.7 and 42.1° for [Cp_2Sn] and [Cp_2Pb], respectively, and are of the same order as the observed values of 45.9−48.4[6b] and 45.5°,[8b] respectively. The above-calculated values indicate that the structure of [Cp_2Sn] has a greater perturbation from the linear situation than that of [Cp_2Pb]. Although there are only small calculated differences in energy between the linear and bent conformers of [Cp_2E], even though these molecules are bent monomers in the gas phase, the observation of bent and almost linear independent molecules in the solid-state structure of [Cp_2Sn] suggests that the energy difference is small enough to be overcome by crystal packing.[6c]

An examination of the individual metal−carbon distances of [Cp_2Sn] reveals that, due to slippage of the metal and inclination of the rings, there are shorter Sn−C lengths (2.56 Å) and longer values (2.91 and 3.09 Å). The metal−carbon bonding will be stronger through the former contacts, which involve the basal carbons. This view is reinforced by a survey of the corresponding carbon−carbon bond lengths in the Cp rings. The bond distances between the basal carbon atoms are longer (1.44 Å), indicative of reduced carbon−carbon bonding, while the remaining carbon−carbon bond lengths span 1.41 and 1.42 Å. A similar pattern is observed for [Cp_2Pb], but here the range of C−Pb distances is narrower (2.71−2.97 Å), as are the related C−C bond values (1.42−1.43 Å). Thus, the small energy differential between the D_{5d} and C_{2v} models of [Cp_2Pb] is related to the similarity of the structures (in the D_{5d} model the Pb−C distances span 2.83 Å and the C−C bond lengths are 1.42 Å).

Analysis of the atomic charges of the most stable structures obtained for the LANL1DZ basis set via Mulliken population analysis reveals that the charges on both metal atoms correspond to a charge of +1, with the Pb having slightly more positive charge (+1.10 e) than Sn (+1.01 e). The corresponding negative charge

(17) (a) Hay, P. J.; Wadt, W. R. *J. Chem. Phys.* **1985**, *82*, 270. (b) Wadt, W. R.; Hay, P. J. *J. Chem. Phys.* **1985**, *82*, 284. (c) Hay, P. J.; Wadt, W. R. *J. Chem. Phys.* **1985**, *82*, 299.

(18) (a) Stevens, W. J.; Basch, H.; Krauss, M. *J. Chem. Phys.* **1984**, *81*, 6026. (b) Stevens, W. J.; Krauss, M.; Basch, H.; Jasian, P. G. *Can. J. Chem.* **1992**, *70*, 612. (c) Cundani, T. R.; Stevens, W. J. *J. Chem. Phys.* **1993**, *98*, 5555. Basis sets were obtained from EMSL Basis Set Library, Molecular Science Computing Facility, Environmental and Molecular Science Laboratory, Pacific Northwest Laboratory, P.O. Box 999, Richland, WA, 99352.

(19) Krishnan, R.; Binkley, J. S.; Seeger, R.; Pople, J. A. *J. Chem. Phys.* **1986**, *72*, 650.

(20) Frisch, M. J.; Trucks, G. W.; Head-Gordon, M.; Gill, P. M. W.; Wong, M. W.; Foresman, J. B.; Johnson, B. G.; Schlegel, H. B.; Robb, M. A.; Replogle, E. S.; Andres, J.; Andres, J. L.; Raghavachari, K.; Binkley, J. S.; Gonzalez, C.; Martin, R. L.; Fox, D.; Defrees, D. J.; Baker, J.; Stewart, J. J. P.; Pople, J. A. Gaussian 92; Gaussian Inc., Pittsburgh, PA, 1992.

(21) Frisch, M. J.; Trucks, G. W.; Schlegel, H. B.; Gill, P. M. W.; Johnson, B. G.; Robb, M. A.; Cheeseman, J. R.; Keith, T.; Petersson, G. A.; Montgomery, J. A.; Raghavachari, K.; Al-Laham, M. A.; Zakrzewski, V. G.; Ortiz, J. V.; Foresman, J. B.; Cioslowski, J.; Stefanov, B. B.; Nonayakkara, A.; Challacombe, M.; Peng, C. Y.; Ayala, P. Y.; Chen, W.; Wong, M. W.; Andres, J. L.; Replogle, E. S.; Gompents, R.; Martin, L. R.; Fox, D.; Binkley, J. S.; Defrees, D. J.; Baker, J.; Stewart, J. J. P.; Head-Gordon, M.; Pople, J. A. Gaussian 94; Gaussian Inc., Pittsburgh, PA, 1995.

Table 7. Orbital Energies (eV) of the Highest Filled MOs of [Cp_2Sn] and [Cp_2Pb][a]

[Cp_2Sn]			[Cp_2Pb]		
calcd values			calcd values		
C_{2v}	D_{5d}	exptl values	C_{2v}	D_{5d}	exptl values
−8.08 ($11b_2$)	−8.06 ($5e_{1g}$)	−7.57	−7.93 ($11b_2$)	−7.93 ($5e_{1g}$)	−7.5
−8.09 ($7a_2$)		−7.91	−7.95 ($7a_2$)		−7.8
−9.16 ($12a_1$)	−9.20 ($5e_{1u}$)	−8.85	−9.09 ($12a_1$)	−9.07 ($5e_{1u}$)	−8.5
−9.30 ($7b_1$)		−8.85	−9.13 ($7b_1$)		−8.8
−10.26 ($11a_1$)	−9.86 ($4a_{1g}$)	−9.58	−11.0 ($11a_1$)	−10.89 ($4a_{1g}$)	−10.1

[a] All energies are from LANL1DZ basis set calculations.

is found on the basal carbon atoms, i.e., those nearest the metal atom. The valence electron populations of Sn and Pb are s 1.98 p_x 0.34 p_y 0.15 p_z 0.51 for Sn and s 2.03 p_x 0.36 p_y 0.14 p_z 0.39 for Pb. Thus, it can be seen that the metal s electrons are not involved in the electron transfer to the Cp rings. The metal p_z orbital lies on the C_{2v} rotation axis, and its occupancy is related to the composition of the lone pair of electrons on the metal. Thus, this lone pair of electrons contains more p_z character in [Cp_2Sn] than in [Cp_2Pb] and this correlates nicely with the greater tilting of the rings and greater ring slippage in [Cp_2Sn]. To observe how the valence electrons are distributed throughout the molecule, we looked at the five highest filled orbitals of [Cp_2E] (the energies are presented in Table 7). The orbital patterns for the [Cp_2E] species are very similar. The two highest bonding orbitals, which are close in energy, are concentrated on the orbitals of the Cp rings and are essentially an antibonding combination of π-orbitals. The next two orbitals, which are also close in energy, involve the interaction of the π-orbitals of the Cp rings with the p_x orbitals of the metal (b_1 symmetry) and the interaction of π-orbitals with the s and p_z orbitals of the metal ($12a_1$ symmetry). The fifth highest orbital ($11a_1$) is localized on the valence s orbital of the metal. Table 7 also contains the corresponding orbital energies of the [Cp_2E] species present in D_{5h} symmetry. It can be seen that the orbital which has been most stabilized by the change in geometry, i.e., the tilting of the rings and slippage of the metal, is $11a_1$. This is especially so for the tin compound, where the gain in stabilization is 0.40 eV. Finally, the experimetal photoelectric spectrum values[22] can be compared to the orbital energies *via* Koopmans' theorem.[23] Satisfactory agreement between the theoretical and experimental values is obtained especially in the trend of the $11a_1$ orbital, which increases in stability on going from [Cp_2Sn] to [Cp_2Pb].

In simple chemical terms the results on [Cp_2Pb] and [Cp_2Sn] illustrate the same trend and orbital pattern as that found for [Cp_2Ge].[24] The latter compound was also subjected to a geometry optimization by the same ECP basis set so that meaningful comparison could be carried out. The results (also presented in Table 6) show an additional and as yet unrecognized feature that the energy difference between the bent (C_{2v}) and linear (D_{5d}) forms of [Cp_2E] diminishes as E goes from Ge (6.4 kcal mol^{-1}) *via* Sn (4.0 kcal mol^{-1}) to Pb (0.7 kcal mol^{-1}). This result can be rationalized in terms of less efficient admixing of the p_z orbital and the s orbital as a result of increased energetic separation of the atomic s and p orbitals. This combining can be correlated with the bending of the rings from the linear situation. Thus, for [Cp_2Ge], where the bending of the rings is the greatest, the occupancy of the valence p_z orbital of Ge is highest (0.61 e).

The next series of calculations looked at the complexes of the [Cp_2E] molecules with [CpNa] (E = Sn (**1′**), Pb (**3′**) (Figure 5), representing models for **1** and **3**, respectively) along with the related separate anions [Cp_3E]$^-$ (E = Sn (**2′**), Pb (**4′**) (Figure 5), representing models for the anions of **2** and **4**, respectively). It was found for these species that it is impossible to achieve a geometry optimization for **1′** using the LANL1DZ basis set. Thus, the SBKJC18 basis set was used to examine the tin compounds while the LANL1DZ basis set was employed for the lead molecules.

The calculated optimized geometry for [Cp_2Sn(μ-Cp)-Na] (**1′**) (Figure 5) shows that the complex is best described as a loose complex of [Cp_2Sn] and [CpNa] rather than as an ion pair of [Cp_3Sn]$^-$ and Na^+. This view is reflected in the presence of two distinct Sn−Cp-(centroid) distances, namely terminal (2.502, 2.509 Å) and bridging (4.092 Å). The former values are similar to the values obtained for [Cp_2Sn]. In a similar manner the Na−Cp centroid distance (2.258 Å) is only slightly longer than the distance found for an isolated [CpNa] species (2.250 Å) using the same basis set. The energy of association of [Cp_2Sn] and [CpNa] is calculated to be 2.84 kcal mol^{-1}, underlining the weak nature of the association. A similar situation is found for the optimized geometry of the corresponding Pb complex **3′**. The weak nature of the interaction between [Cp_2Pb] and [CpNa] is reflected in the longer bridging Pb−Cp centroid distance (3.588 Å) and the shorter terminal Pb−Cp distance. The Na−Cp centroid distance in **3′** has only marginally increased (0.02 Å) due to complexation, and there is only a small electron transfer (0.01 e) from the [CpNa] moiety to the [Cp_2Pb] portion. The calculated energy of association is 4.5 kcal mol^{-1}.

The most notable difference between the theoretical structures of [Cp_2E(μ-Cp)Na] (E = Sn (**1′**) and Pb (**2′**)) and the crystal structures (**1** and **3**) is that the bridging and terminal E−Cp centroid distances are considerably smaller in the experimental structures. This discrepancy must be due to the effect of Lewis base solvation of the Na^+ cations in the X-ray structures (cf. the theoretical structures **1′** and **3′**, which are unsolvated). In order to examine this effect further, [Cp_2Sn(μ-Cp)-$NaNH_3$] (**1a′**) was examined theoretically. It was found that the effect of the inclusion of NH_3 was to lengthen (i.e., weaken) the Na−Cp distance (2.295 Å) and to move

(22) (a) Bruno, G.; Ciliberto, E.; Fragala, J. L.; Jutzi, P. *J. Organomet. Chem.* **1985**, *289*, 263. (b) Baxter, S. G.; Cowley, A. H.; Lasch, J. G.; Lattman, M.; Sharum, W. P.; Steart, C. A. *J. Am. Chem. Soc.* **1982**, *104*, 4064.

(23) Koopmans, T. *Physica* **1933**, *104*, 1064.

(24) Almløf, J.; Fernholt, L.; Faegri, K., Jr.; Haaland, A.; Schilling, B. E. R.; Seip, R.; Tangol, K. *Acta Chem. Scand.* **1983**, *A37*, 131.

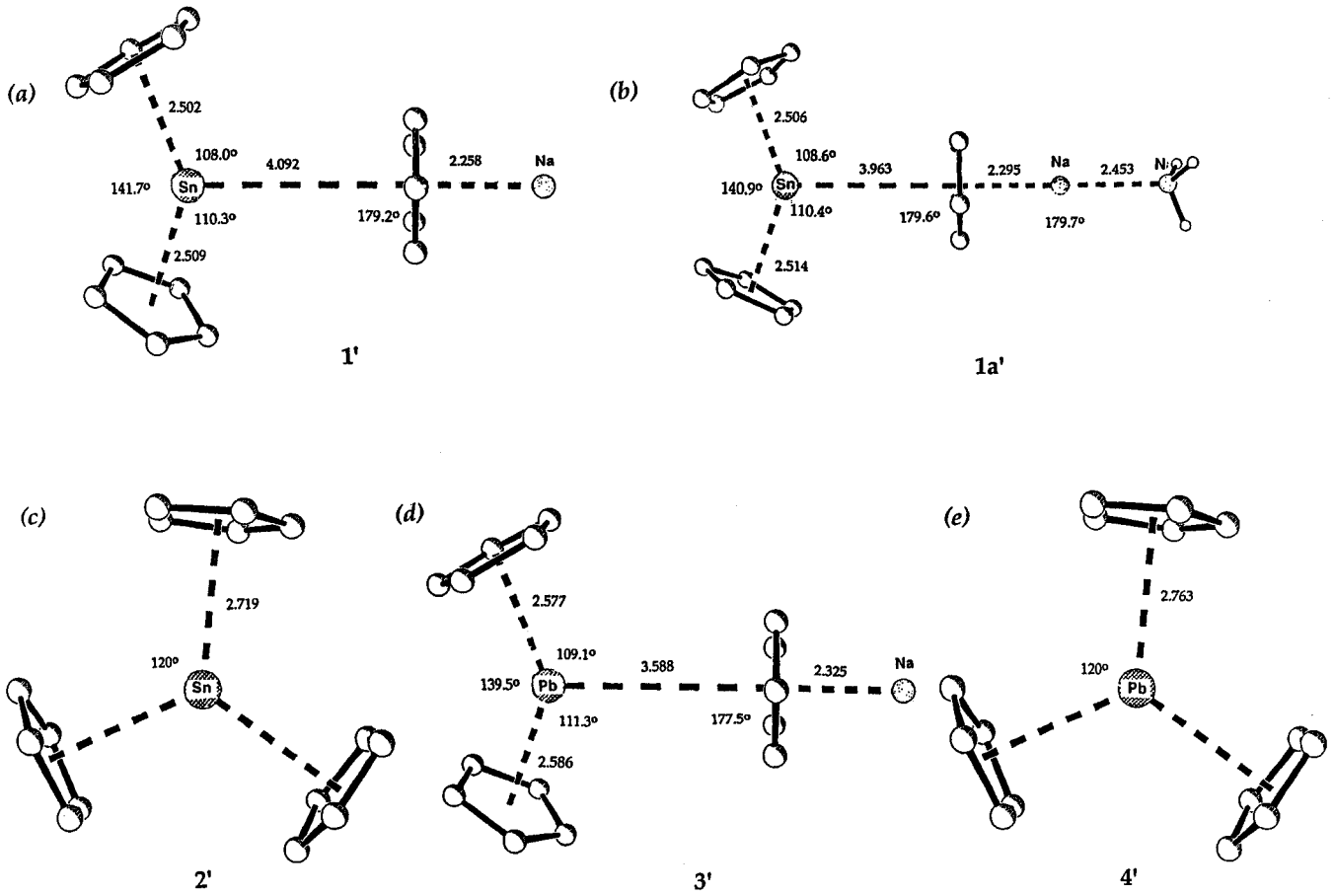

Figure 5. *Ab initio* optimized geometries of Sn and Pb complexes (basis sets used and absolute energies (au) in parentheses): (a) $[Cp_2Sn(\mu\text{-}Cp)Na]$ (**1′**) (SBKJC18, −741.948 098); (b) $[Cp_2Sn(\mu\text{-}Cp)NaNH_3]$ (**1a′**) (SBKJC18, −798.184 566); (c) $[Cp_2Pb(\mu\text{-}Cp)Na]$ (**2′**) (LANL1DZ, −6570.1684); (d) $[Cp_3Sn]^-$ (**3′**) (SBKJC18, −580.086 156); (e) $[Cp_3Pb]^-$ (**4′**) (LANL1DZ, −579.8822).

the bridging Cp ligand into closer contact (by 0.13 Å) with Sn. The calculated energy of association of NH_3 with **1′** is 17.2 kcal mol^{-1}, underlining the significance of this interaction. It is not too difficult to envisage that the effect of a strong multidentate Lewis base donor such as PMDETA will be to weaken the Na−Cp distance further and to move the bridging Cp into closer contact with Sn. The calculational results on the loose-contact Sn model, i.e., $[Cp_2Sn.CpNa]$ (**1′**), can be compared to those of a calculation in which the Na is bonded directly to Sn with the Cp rings arranged in a pyramidal fashion about the Na−Sn bond axis (C_3 symmetry) and with the Cp rings arranged in a pyramidal fashion about the Na−Sn bond axis. The latter model was found to be substantially (47.9 kcal mol^{-1}) less stable than **1′**, and this appears to rule out the possibility of metal-metal bonding occurring in these particular compounds.

The structures of isolated $[Cp_3E]^-$ represent a situation in which the cations have been removed by the effect of Lewis base solvation. The optimized geometries were performed with C_{3h} symmetry, giving the classical paddle-wheel geometries of the ion-separated species, with the three Cp ligands being attached equivalently to the Sn and Pb centers. The metal−Cp(centroid) distances of 2.719 and 2.763 Å for $[Cp_3Sn]^-$ (**2′**) and $[Cp_3Pb]^-$ (**4′**) (Figure 5), respectively, have increased from the values found for Cp_2E and are close to the experimental distances found in the solid-state structures of the ion-separated complexes **2** and **4**. The energies of association of Cp^- with $[Cp_2E]$ are calculated to be 22.7 and 30.6 kcal mol^{-1} for E = Sn, Pb, respectively. These values are greater than the corresponding energies of association of [CpNa] and $[Cp_2E]$ and reflect the greater Lewis basicity of Cp^- and hence the increase in bonding of the Cp ring with the metal orbitals.

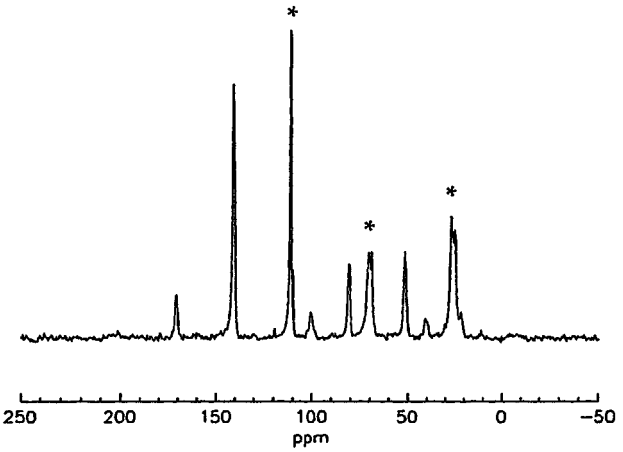

Figure 6. Solid-state ^{13}C CP/MAS NMR (^1H decoupled) spectrum of **2** (+25 °C, relative to TMS; asterisks denote the actual resonances).

Solid-State NMR Spectroscopy. The magic-angle spinning ^{13}C NMR (MAS) spectrum of **2** recorded with cross-polarization (CP) and ^1H decoupling at room temperature is shown in Figure 6. The spectrum varies very little with temperature between −150 and +40 °C.

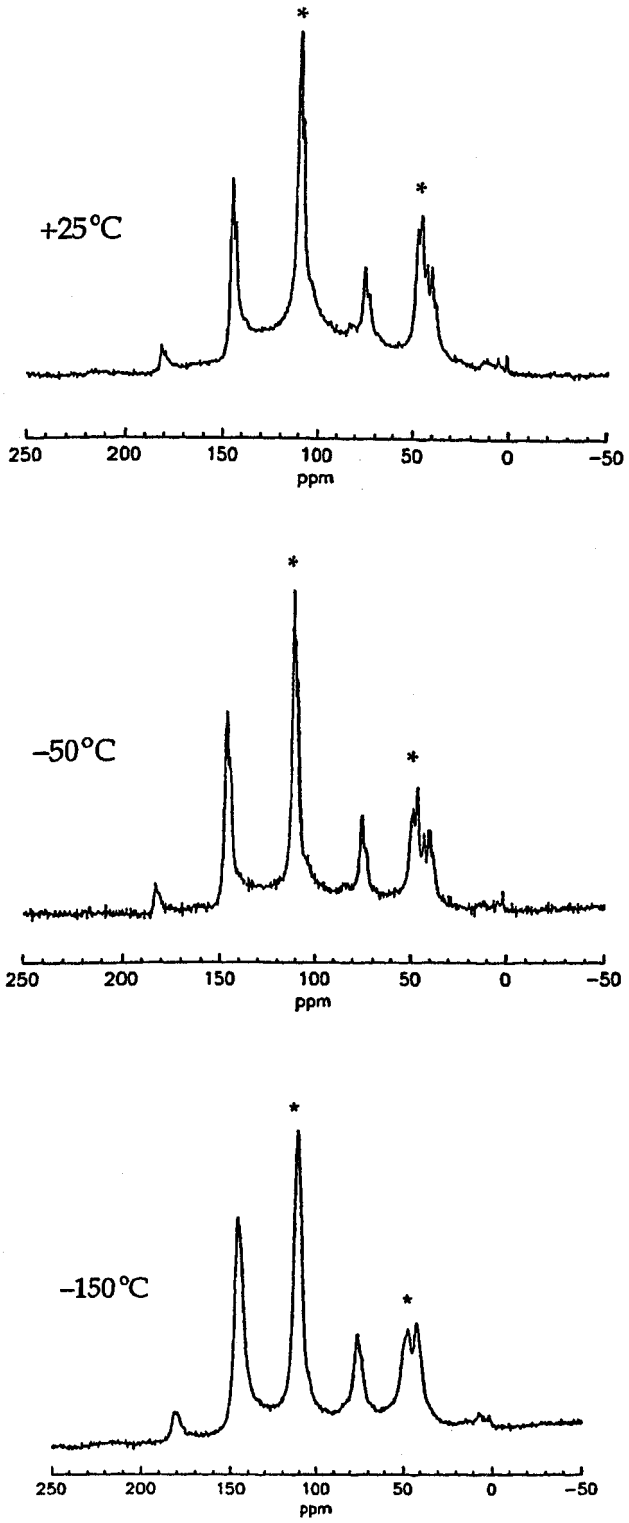

Figure 7. Solid-state ^{13}C CP/MAS NMR (^{1}H decoupled) spectra of **1** (relative to TMS, asterisks denote the actual resonances).

The resonance at 111.7 ppm (relative to TMS) is due to the cyclopentadienyl carbons, which is flanked by a number of spinning sidebands arising from the non-zero chemical shift anisotropy associated with these ^{13}C spins. Peaks at 67 and 24 ppm are due to Mg-attached THF ligands.

The most obvious feature of this spectrum is that there is only one ^{13}C Cp signal. Thus, not only are all three cyclopentadienyl rings equivalent (as shown by X-ray diffraction results) but they must also undergo rapid rotational motion which makes all the ^{13}C sites equivalent on the NMR time scale. Further evidence for the rapid spinning of the Cp ligands about their approximate 5-fold axes comes from analysis of the spinning sidebands in the ^{13}C NMR spectrum. The sideband pattern can be simulated with an effective chemical shift anisotropy of 119 ± 10 ppm and an asymmetry of 0; i.e., the chemical shift tensor has axial symmetry. The symmetry of the ^{13}C sites in the Cp igands is not axial, and so in the absence of any motional averaging, one would expect a nonaxial chemical shift tensor, i.e., non-zero asymmetry. The axial chemical shift tensor actually observed is the result of rapid rotational motion about a single axis. This motion also has an effect on the chemical shift anisotropy, in this case reducing the anisotropy to roughly half of the static value.[25]

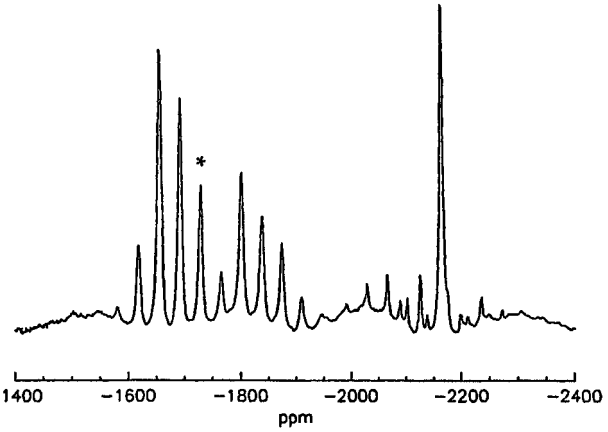

Figure 8. Solid-state ^{119}Sn CP/MAS NMR (^{1}H decoupled) spectrum of **2** (+25 °C, relative to $SnCl_2$, the asterisk denotes the actual resonance).

The ^{13}C CPMAS NMR spectra of **1** recorded between −150 °C and room temperature are shown in Figure 7. The signal at 111 ppm, flanked by spinning sidebands, is due to the Cp ligands, and those occurring below 50 ppm (other than the Cp spinning sidebands) are due to the PMDETA ligand. These spectra exhibit a marked temperature dependence in their line widths, with the lowest temperature spectrum being rather poorly resolved as a result. Indeed, even the narrowest line widths (recorded at room temperature) are significantly larger than those in the ^{13}C NMR spectra of **2**. The uniformity of the line broadening at low temperature suggests that it arises from static disorder, an inhomogeneity which affects the whole sample, rather than from a localized molecular motion which could also cause line broadening at certain speeds of motion.

Interestingly, in the ^{13}C NMR spectrum of **1** at −50 °C the linewidths have narrowed sufficiently and three closely spaced isotropic Cp peaks are resolved at 112.2, 111.4, and 110.2 ppm. These arise from the three crystallographically different Cp environments present in the complex: the μ-Cp ligand and the two terminal Cp ligands, one of which is involved in an agostic interaction with a neighbouring molecule. On the basis of the ^{13}C chemical shift observed in [CpLi] (102 ppm),[26] in which the Cp ligands are approximately "free" Cp^-, we can assign the lowest frequency resonance at 110.2

(25) Wittebort, R. J.; Olejniczak, E. T.; Griffin, R. G. *J. Chem. Phys.* **1987**, *86*, 5411.
(26) Ford, T. J. *Am. Chem. Soc.* **1974**, *96*, 309.

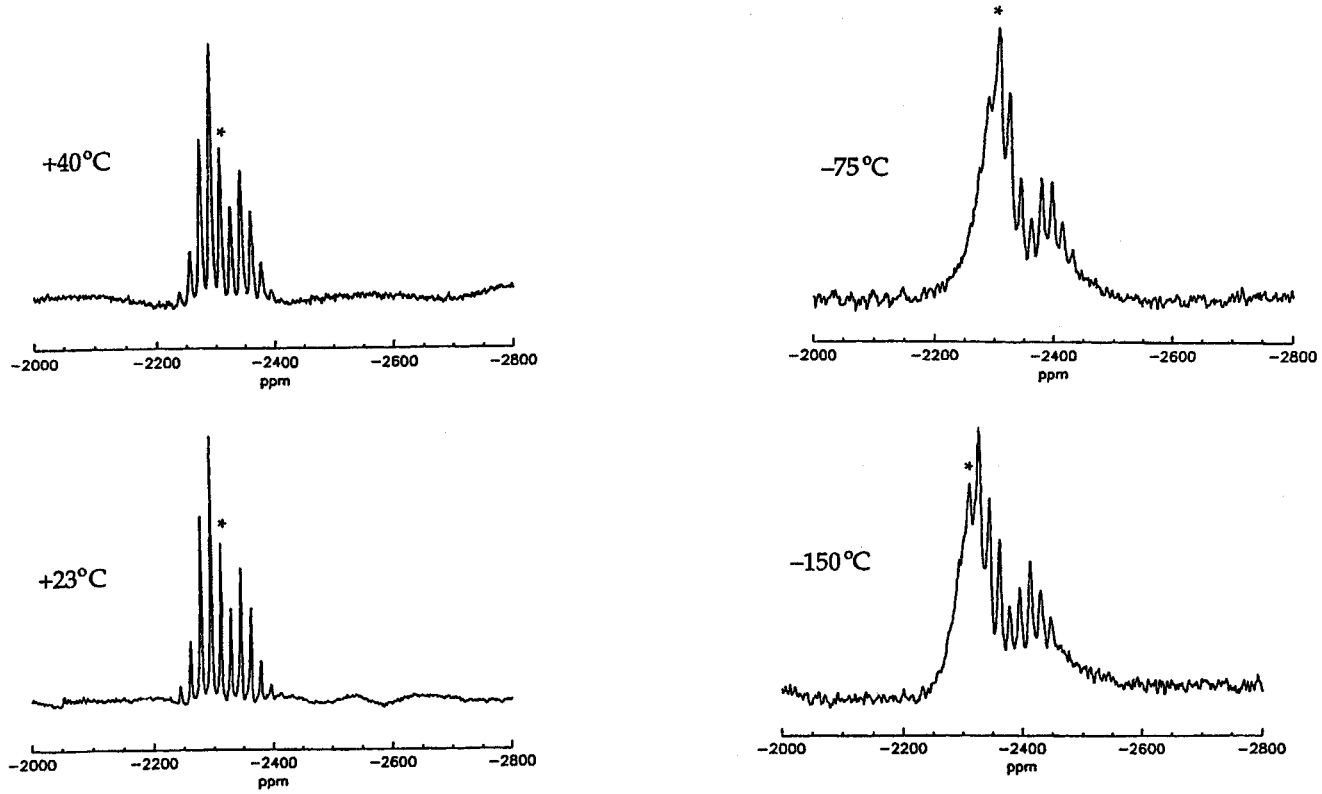

Figure 9. Solid-state ^{119}Sn CP/MAS NMR (^{1}H decoupled) spectra of **1**, (relative to $SnCl_2$, asterisks denote the actual resonances).

ppm to the μ-Cp ligand A, that at 111.4 ppm to the Cp ring B, and that at 112.2 ppm to the remaining terminal Cp ring C (Figure 1). Further reductions in line width occur with increasing temperature, but despite this only two Cp signals, at 111.9 (terminal Cp) and 109.8 ppm (μ-Cp), are observed at room temperature in the intensity ratio 2:1, respectively. Clearly, the two terminal Cp ligands have now become equivalent, presumably through some motional process. Analysis of the spinning sidebands associated with the Cp resonances gives a chemical shift anisotropy of 119 ± 10 ppm and an asymmetry of 0 for both. These values agree well with those found for **2** and again demonstrate that all the Cp rings are spinning rapidly about their C_5 axes.

The ^{13}C chemical shifts for the Cp ligands in **1** and **2** reflect a degree of electron donation to the Sn centers from the Cp ligands greater than that which occurs to the metal in [CpLi] (102 ppm). It is interesting to note that in **2** the ^{13}C isotropic chemical shift of the Cp ligands (111.7 ppm) is lower than that found in $[Cp_2Sn]$ (112.6 ppm).[27] This suggests that the Cp ligands in $[Cp_3Sn]^-$ donate less electron density to Sn than those in Cp_2Sn. This is consistent with the *ab initio* MO calculations on these species (see Calculations).

To investigate further the different electron distributions in the ion-paired and free $[Cp_3Sn]^-$ anions of **1** and **2**, ^{119}Sn NMR spectra of both compounds were recorded over a range of temperatures. Figure 8 shows the room-temperature ^{119}Sn NMR spectrum of **2**, in which a single Sn resonance at −1730 ppm, flanked by spinning sidebands, is observed. Simulation of the complete sideband pattern gives a chemical shift anisotropy of 45 kHz and an asymmetry of 0. The chemical shift, chemical shift anisotropy, and asymmetry of the ^{119}Sn signal in **2** are markedly different from those in $[Cp_2Sn]$ (−2199 ppm, 24.5 kHz, and 0.65, respectively).[27] Clearly the chemical and electronic environment of the Sn in **2** is very different from that in $[Cp_2Sn]$.

As with the corresponding ^{13}C NMR spectra, the ^{119}Sn MAS NMR spectra of **1** exhibit a significant increase in line widths at low temperature, presumably due to a static disorder at these temperatures. Figure 9 shows the ^{119}Sn NMR spectra of **1** recorded at various temperatures and spinning speeds.

The ^{119}Sn isotropic chemical shift of −2312 ppm is very similar to the value found for $[Cp_2Sn]$. Analysis of the spinning sidebands gives a chemical shift anisotropy of 117.6 ppm (17.5 kHz) and asymmetry of 0.5, which are again similar to the values obtained previously for $[Cp_2Sn]$ (24.5 kHz and 0.65, respectively). Thus, it appears that, electronically at least, the $[Cp_3Sn]^-$ moiety in the ion-contacted complex **1** is much more like $[Cp_2Sn]$ than that in the ion-separated anion of **2**. These results are entirely consistent with the view of **1** as being more like a "loose-contact" complex of the neutral components $[Cp_2Sn\cdots Cp{-}NaPMDETA]$. This view is again broadly consistent with *ab initio* MO calculations on models of **1** (see Calculations).

Conclusions. Addition of weakly nucleophilic Cp^- anions occurs to $[Cp_2E]$ (E = Sn, Pb) and produces complexes containing essentially planar $[Cp_3E]^-$ anions. However, the nature of the triorgano Sn and Pb species produced is highly dependent on the extent of solvation of the alkali- or alkaline-earth-metal cations (M) involved. Calculational studies illustrate that in the absence of cation solvation these species should be regarded as *loose-contact* complexes ($[Cp_2E\cdots Cp{-}M]$). In the extreme situation of ion separation, where there

(27) Wrackmeyer, B.; Kupce, E.; Kehr, G.; Sebald, A. *Magnetic Resonance in Chemistry*; **1992**, *30*, 964.

is no cation competition for Cp^- electron density (as in **2** and **4**), the species are "genuine" triorganometal anions $[Cp_3E]^-$. Where partial solvation of the cation coordination sphere occurs (as in **1** and **3**), the complexes are partway between the two extremes. These findings are also in broad agreement with solid-state MAS NMR studies on these species.

Theoretical calculations of the parent metallocenes $[Cp_2E]$ (E = Ge, Sn, Pb) show that the preference for the bent conformation is dictated by the energetic separation of the s and p orbitals and hence their ability to admix. This situation also appears to be the case for other 14e metallocenes such as the $[Cp_2Tl]^-$ anion, which we recently characterized.[28]

Experimental Section

General Considerations. $[Cp_2Sn]$ and $[Cp_2Pb]$ and complexes **1**−**4** are highly air- and moisture-sensitive and were prepared under dry O_2-free argon using standard inert-atmosphere techniques.[29] Solvents (THF, toluene) were freshly distilled over Na/benzophenone prior to reactions. PMDETA was used as supplied (Lancaster) after being dried using molecular sieves (13X). $[Cp_2Sn]$ and $[Cp_2Pb]$ were prepared by the reactions of [CpNa] (2 equiv) with $SnCl_2$ (in THF)[6a] and $Pb(NO_3)_2$ (in DMF),[8a] respectively, in the manner described by Fischer and Gruber. They were purified by sublimation at 125 °C for $[Cp_2Sn]$ (up to 90%) and 145 °C for $[Cp_2Pb]$ (up to 60% yield) (both at 0.1 atm).[30] Both complexes are thermally unstable, and $[Cp_2Sn]$ is best stored as a standardized THF solution at −35 °C and $[Cp_2Pb]$ as a solid at the same temperature. Syntheses were carried out in Schlenk tubes on a vacuum line, and dry samples for analytical, infrared, cryoscopic, and NMR work were handled using a glovebox (Faircrest Mark 4A) fitted with a recirculation system (Type B). Elemental compositions (C, H, N) were determined using a Perkin-Elmer 240 elemental analyzer. Samples were sealed in air-tight aluminum boats prior to analysis. Infrared spectra (recorded as Nujol mulls) were prepared in the glovebox and were recorded on a Perkin-Elmer spectrophotometer. Cryoscopic molecular mass measurements were performed using a specially designed apparatus which allowed accurate measurements to be made under argon.[31] Special grade cryoscopic benzene was used and was dried using molecular sieves.[32] NMR samples were sealed in airtight screw-cap NMR tubes (Wilmad, 528pp) in the glovebox and were run on a Bruker WH250, WH360, or WH400 NMR spectrometer. ^{1}H NMR samples were referenced to the internal solvent peaks (C_6D_6, C_6D_5H at δ 7.16 ppm; $C_6D_5CD_3$, $C_6D_5CD_2H$ at δ 2.10 ppm; d_8-THF, C_4D_7HO at δ 3.60 and 1.70 ppm). Basic NMR characterizations were performed at lower field (250 MHz), and these data are given with the synthesis of each complex. Specific higher field experiments (360 and 400 MHz) are included in the Results and Discussion.

Synthesis of $[(\eta^5\text{-Cp})_2\text{Sn}(\mu\text{-Cp})\text{NaPMDETA}]$ (1). [CpNa] (1.25 mL, 2.0 mol L^{-1} in THF, 2.5 mmol) was added to a solution of $[Cp_2Sn]$ (0.623 g, 2.5 mmol) (the preparation is given in ref 6a) and PMDETA (0.53 mL, 2.5 mmol) in THF (5 mL) at 20 °C under nitrogen. Stirring the reaction mixture (0.5 h) at 20 °C gave an orange-red solution. The THF was removed under vacuum and replaced with toluene (5 mL), and the solution was filtered to remove a faint precipitate. Storage of the orange-red filtrate at 20 °C gave air-sensitive light yellow crystalline rods of **1**. First batch yield: 20% (0.26 g, 0.51 mmol). Mp: 93−98 °C to a yellow oil. IR (Nujol mull): ν 3079, 3061 cm^{-1} (C−H str, η^5-Cp),[33] disappears on air exposure. Anal. Found: C, 56.5; H, 7.3; N, 8.3. Calcd: 56.5, H, 7.5; N, 8.2. ^{1}H NMR (+25 °C, 250 MHz, d_6-benzene): δ 6.00 (s, 15H; η^5- and μ-Cp), 1.80 (s, 15H; CH_3−N and $(CH_3)_2$N−), 1.65 (s, 8H; $(CH_2)_2$). Cryoscopic molecular mass (benzene): $[(\eta^5\text{-Cp})_2\text{Sn}(\mu\text{-Cp})\text{NaPMDETA}]_n$, $n = 0.49 \pm 0.02$ (0.015 mol L^{-1}), $n = 0.51 \pm 0.02$ (0.03 mol L^{-1}).

Synthesis of $[(\eta^3\text{-Cp})_3\text{Sn}^-]_2[\text{Mg(THF)}_6]^{2+}$ (2). $[Cp_2Mg]$ (Strem, 0.308 g, 2 mmol) was dissolved in 25 mL of THF, to which was added $[Cp_2Sn]$ (1.00 g, 4 mmol) at 20 °C. The slightly cloudy solution was filtered, and to the filtrate was added a further 5 mL of THF. Storage at 20 °C (24 h) gave colorless cubic crystals of **2**. Crystals of **2** contain one molecule of THF solvate per formula unit; this is removed by placing the complex under vacuum (*ca.* 10^{-2} atm, 15 min). The following analytical and spectroscopic data were obtained on the dry unsolvated powder. First batch yield: 42% (0.92 g, 0.85 mmol). Mp: 57−60 °C to a colorless oil. IR (Nujol mull): ν 3075 cm^{-1} (C−H str, Cp),[33] disappears on air exposure. Anal. Found: C, 58.6; H, 7.4. Calcd: C, 59.7; H, 7.2. ^{1}H NMR (+25 °C, 250 MHz, d_8-THF): δ 5.26 (s, 30H; Cp), *ca.* 3.30 (m, 24H, THF), *ca.* 1.45 (m, 24H, THF).

Synthesis of $[(\eta^5\text{-Cp})_2\text{Pb}(\mu\text{-Cp})\text{NaPMDETA}]$(3). [CpNa] (1.0 mL, 2.0 mol L^{-1} in THF, 2.0 mmol) was added to a solution of $[Cp_2Pb]$ (0.674 g, 2.0 mmol) (preparation is given in ref 8a) and PMDETA (0.35 mL, 2.0 mmol) in THF (5 mL) at 20 °C under argon. The bright orange solution produced was concentrated by removing *ca.* 1 mL of solvent under vacuum, and the resulting solution was refrigerated (12 h) at 5 °C. A crop of bright yellow crystalline blocks of **3** were produced. First batch yield: 26% (0.31 g, 0.52 mmol). Mp: 146−149 °C to a bright yellow oil. IR (Nujol mull): ν 3077 cm^{-1} (C−H str, η^5-Cp),[33] disappears on air exposure. Anal. Found: C, 47.5; H, 6.4; N, 6.9. Calcd: 48.1; H, 6.4; N, 7.0. ^{1}H NMR (+25 °C, 250 MHz, d_8-THF): δ 5.28, 5.27 (s, 15H; Cp), 2.07 (m, 8H; $(CH_2)_2$), 1.91 (s, 3H; CH_3−N), 1.87 (s, 12H; $(CH_3)_2$N−). Cryoscopy in benzene: $n = 0.47 \pm 0.04$ (0.005 mol L^{-1}).

Synthesis of $[(\eta^3\text{-Cp})_3\text{Pb}^-]_2[\text{Mg(THF)}_6]^{2+}$ (4). Cp_2Mg (Strem, 0.308 g, 2 mmol) was dissolved in 6 mL of THF to which was added Cp_2Pb (1.00 g, 4 mmol) at 20 °C. The reaction mixture was stirred for 1 h at 25 °C, and a mass of yellow powder was formed. The solid was dissolved by gentle heating, and the yellow solution produced was stored at 20 °C (24 h) to give yellow cubic crystals of **4**. Crystals of **4** contain one molecule of THF solvate per formula unit, this is removed by placing the complex under vacuum (*ca.* 10^{-2} atm, 15 min). The following analytical and spectroscopic data were obtained on the dry unsolvated powder. First batch yield: 59% (1.49 g, 1.18 mmol). Mp: darkens at *ca.* 95 °C and melts at 125 °C. IR (Nujol mull): ν 3076 cm^{-1} (C−H str, Cp),[33] disappears on air exposure. Anal. Found; C, 51.2; H, 6.0. Calcd: C, 51.4; H, 6.2. ^{1}H NMR (+25 °C, 250 MHz, d_8-THF): δ 5.76 (s, 30H; Cp), *ca.* 3.38 (m, 24H, THF), *ca.* 1.32 (m, 24H, THF).

X-ray Structure Determinations of 1−4. Crystals were mounted directly from solution under Ar using a perfluorocarbon oil, which protects them from atmospheric O_2 and moisture. The oil "freezes" at reduced temperatures and holds

(28) Armstrong, D. R.; Herbst-Irmer, R.; Kuhn, A.; Moncrieff, D.; Paver, M. A.; Russell, C. A.; Stalke, D.; Steiner, A.; Wright, D. S. *Angew. Chem.* **1993**, *105*, 1807−1810; *Angew. Chem., Int. Ed. Engl.* **1993**, *32*, 1774−1777.

(29) Shriver, D. F.; Dredzon, M. A. *The Manipulation of Air-Sensitive Compounds*, 2nd ed.; Wiley: New York, 1986.

(30) Health and safety note: both complexes are highly toxic, and contact with skin or inhalation should be avoided. Particular care should be taken in disposing of the black residue produced after sublimation of $[Cp_2Pb]$. Air exposure can lead to spontaneous ignition in an extremely exothermic reaction followed by explosion. Do not try and fight the fire (rather like the back of a jet engine). Careful addition of water under an inert atmosphere followed by air exposure is recommended. Preparations over 0.2 mol should be avoided. Alternatively, use $[Pb(AcO)_2]$ instead of $[Pb(NO_3)_2]$.

(31) Davidson, M. G.; Snaith, R; Stalke, D.; Wright, D. S. *J. Org. Chem.* **1993**, *58*, 2810.

(32) Acquired from Fisons Scientific Equipment, Bishops Meadow Road, Loughbourgh, Leicestershire LE11 0RG, U.K.

(33) This band is particularly characteristic in complexes **1**−**4** and in related compounds.

the crystals static in the X-ray beam.[34] Data were collected on a Stoe-Siemens AED diffractometer, and semiempirical absorption corrections based on ψ scans were employed for all the complexes. Relevant details of the structure refinements of complexes **1**−**4** are given in Table 1. Key bond lengths and bond angles for these compounds are shown in Tables 2−5. All structures were solved by direct methods (SHELX TL PLUS) and refined by full-matrix least squares on F^2.[35] Atomic coordinates, bond lengths and angles, and thermal parameters for **1**−**4** have been deposited with the Cambridge Crystallographic Data Centre.

Solid-State MAS/NMR Spectroscopy. All solid-state NMR spectra were recorded on a Chemagnetics CMX-400 spectrometer. All were recorded under magic-angle spinning (MAS). Samples were sealed under nitrogen in zirconia rotors. At a given temperature, spectra were routinely recorded at several different spinning speeds, the spinning speed being actively stabilized to within ±5 Hz. Analyses of spinning sidebands use data from at least two different spinning speeds. In the case of the ^{119}Sn spinning-sideband analysis, more than three spinning speeds were generally used. Spinning sideband analyses involve simulation of the entire sideband pattern[36] for trial values of the principal values of the chemical shift tensor until an acceptable "eyeball" fit is obtained.

^{13}C NMR spectra were recorded at 100.57 MHz with a ^{1}H decoupling field of 50 kHz at 399.906 MHz during acquisition. Cross-polarization was not used, as quantitative sideband intensities were required. The ^{13}C 90° pulse length was 5 ms; the recycle delay was 5 s. Over 700 scans were collected for each spectrum. ^{119}Sn NMR spectra were recorded at 148.79 MHz with ^{1}H decoupling of 50 kHz during acquisition. The ^{119}Sn 90° pulse was 2.3 ms; the recycle delay was 5 s. Over 300 scans were collected for each spectrum.

Acknowledgment. We gratefully acknowledge the EPSRC (M.J.D., C.A.R., C.S., D.S.W.), the Associated Octel Co. Ltd. (D.S.W.), the Nuffield Foundation (D.S.W.), the Royal Society (D.S.W.), Sidney Sussex College (Fellowship for C.A.R.), St. John's College (M.J.D.), and the Deutsche Forschungsgemeinschaft and the Fonds der Chemischen Industrie (D.S., A.S.), for financial support. D.M. also thanks the U. S. Department of Energy through Contract No. DE-FC05-85ER-2500000 and the U. S. Department of Energy and Chemical Science through Contract No. DE-FG05-95ER-14523. We also thank Mr. Steve Wilkinson (Cambridge) for running NMR spectra and for technical support.

Supporting Information Available: Tables giving crystal data and details of the structure determinations, bond lengths, bond angles, anisotropic displacement coefficients, and atom coordinates and isotropic displacement parameters for **1**, **2**, and **4** (14 pages). Ordering information is given on any current masthead page.

OM970161K

(34) Stalke, D.; Kottke, T. *J. Appl. Crystallogr.* **1993**, *26*, 615.
(35) Sheldrick, G. M. SHELX-93; University of Göttingen, Göttingen, Germany, 1992.
(36) Maricq. M. M.; Waugh, J. S. *J. Chem. Phys.* **1979**, *70*, 3300. Herzfeld, J.; Berger, A. E. *J. Chem. Phys.* **1980**, *73*, 6021.